

Artificial circumzenithal and circumhorizontal arcs

Markus Selmke^{a)} and Sarah Selmke
Universität Leipzig, 04103 Leipzig, Germany

(Received 9 July 2016; accepted 18 May 2017)

A glass of water, with white light incident upon it, is typically used to demonstrate a rainbow. On a closer look, this system turns out to be a rather close analogy of a different kind of atmospheric optics phenomenon altogether: circumzenithal and the circumhorizontal halos. The work we present here should provide a missing practical demonstration for these beautiful and common natural ice halo displays. © 2017 American Association of Physics Teachers.
[<http://dx.doi.org/10.1119/1.4984802>]

I. INTRODUCTION

Light that falls onto a transparent thin-walled cylinder (such as a drinking glass) filled with water gets refracted.^{1,2} Several ray paths may be realized through what then effectively represents a cylinder of water. Light can either illuminate and enter through the side of the cylinder, or it can enter through the top or bottom interfaces, depending on its origin and direction of travel. Indeed, the former situation (illumination from the side and under a shallow inclination angle) reveals a rainbow in the backward direction. The reason for the backward rainbow being that the geometry mimics the incidence plane geometry of a light path through a spherical raindrop: refraction, internal reflection, and a second refraction upon exit, all occurring at the cylinder's side wall, produce the familiar observable rainbow caustic in the backward direction at around 42° from the incident light source.³⁻⁶

Now, returning to the initial claim, we consider illumination of the glass through the top water-air interface. If the angle of incidence is shallow enough, light may exit through the cylinder's side wall. Contrary to common belief,^{1,2} (cf. also blogs, etc., found via an internet search for “glass water table rainbow”), this situation is *not* related to the rainbow. Instead, this geometry equals the *average* geometry of light paths through an upright hexagonal ice prism, entering through the (horizontal) top face and leaving through either of its six (vertical) side faces, as shown in Fig. 1. The averaging is meant to be over different prism orientations as indicated in the figure; this, in turn, is what typically causes the natural atmospheric phenomenon known as the circumzenithal arc (CZA) halo,⁶⁻¹⁵ an example of which is shown in Fig. 2(a). In the experiment, an analogous curved spectrum is observed when the refracted light is projected on the floor (the horizontal plane) some distance from the cylinder,¹⁶ as shown in Fig. 2(b).

Similarly, illuminating the glass at a very steep angle at its side, the light may enter through the side wall and leave through the top surface. Now, apart from top and bottom being reversed, this geometry equals the *average* geometry of light entering a rectangular (vertical) side face of a hexagonal plate crystal and leaving through its bottom (horizontal) hexagonal face. This is the situation corresponding to the natural halo phenomenon known as the circumhorizontal arc (CHA).^{6-10,12-15}

Anecdotally, it is puzzling why Huygens, who was the first to establish an extensive quantitative framework for halos based on the (false) assumption of refracting cylinders, did not conceive of this CZA mechanism and instead invoked a more complicated one.^{16,17}

We will detail each experimental setup and show how to arrive at a quantitative description of several aspects of the artificial halo analog, re-deriving well-known expressions from the natural atmospheric optics ice-halo phenomena. For ideal experimental results, one can use a round reflection cuvette. However, a beaker (e.g., borrowed from a French coffee press) or any other cylindrical glass and a focusable LED flashlight or a projector lamp (a bright source of *parallel* white light) will work just fine.

II. ARTIFICIAL CIRCUMZENTHAL ARC

We begin with the artificial CZA, for which a ray is assumed to enter through the top air-water interface and to leave the cylinder through its side wall, as depicted in Figs. 3(a)–3(c). At the first interface, the ray changes its inclination angle e toward the horizontal plane according to Snell's law. We denote complementary angles by a subscript c , such that, for instance, $e_c = \pi/2 - e$ [see Fig. 3(b)]. Thus, taking $n = 1$ for air we have $\sin e_c = n_0 \sin e'_c$, with an associated transmission coefficient $T_1(e_c)$ according to the Fresnel equations. When later discussing intensities, we will consider polarization-averaged transmission coefficients only, although this approach will not strictly be valid for the second refraction due to the partial polarization upon the first refraction.

The second (skew-ray) refraction now occurs under a geometry that may be decomposed into two parts.^{12-15,19,20} One is in the horizontal plane, shown from the top in Fig. 3(c), and described by an effective index of refraction n' (Bravais' index of refraction for inclined rays) given by²¹

$$n' = \sqrt{\frac{\cos^2 e'}{1/n_0^2 - \sin^2 e'}} \quad (1)$$

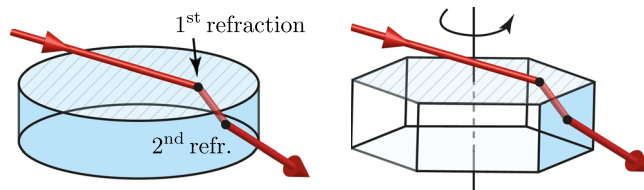


Fig. 1. First refraction: Rays entering through the top face (faintly ruled) of both a cylinder (left) and a hexagonal prism (right) experience an equal inclination refraction. Second refraction of the skew rays by the side faces in both cases are equivalent when the effect of rotational averaging of the prism is considered. The same holds true for the reverse ray paths.

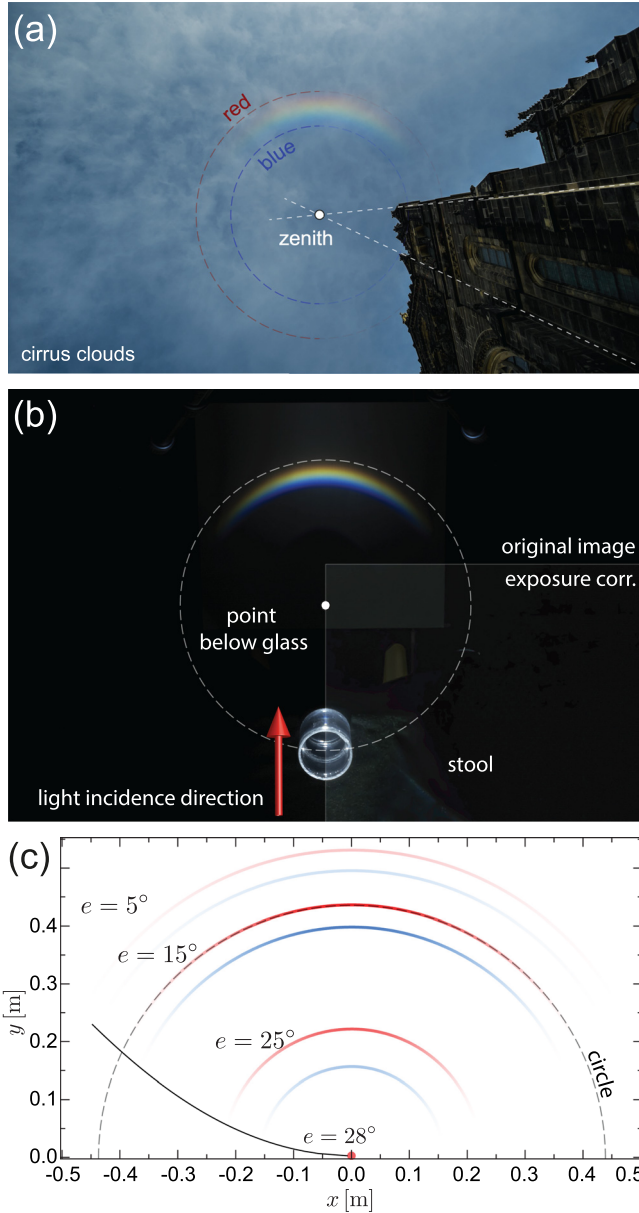


Fig. 2. (a) Natural circumzenithal arc (CZA) halo display. The solar elevation was $e = 27^\circ$ (Ref. 22), and the angular distance to the zenith was $e'' = 16^\circ$ as determined with the help of the vanishing lines of vertical and parallel features of the building (dashed lines) (Ref. 23). (b) Artificial CZA produced by illuminating the top surface of a water-filled acrylic cylinder under a shallow angle (outer diameter: 50 mm, inner diameter: 46 mm, length: 50 mm, height: $l = 1$ m). (c) Artificial CZA curves according to Eq. (3) for $e = \{5^\circ, 15^\circ, 25^\circ\}$ and for red and blue color each. Shading according to the intensity $I(\phi'')$, given in Eq. (6). Full color-spectrum versions are described in Appendix A.

There is also a second inclination refraction described by the actual material's index of refraction n_0 . The exiting ray, which hits the cylinder's side wall under an xy -projected incidence angle of ϕ (to the normal), is thus deflected in the horizontal plane by $\phi'' = \phi' - \phi$, where Snell's law connects the latter two angles via $n' \sin \phi = \sin \phi'$. The inclination angle to the plane changes according to $n_0 \sin e' = \sin e''$, such that overall the exit angle to the vertical becomes^{11–13,15}

$$e''_c = \arccos(\sqrt{n_0^2 - \cos^2 e}). \quad (2)$$

Referring to the experiment's setup and coordinates as defined in Fig. 3(a), one finds for each light source

inclination angle e the deflected rays to lie on a curve $(x(\phi), y(\phi))$. We will neglect the finite size of the glass as an approximation and thereby assume its diameter \varnothing to be much smaller than the vertical distance l to the surface onto which the ray is projected ($\varnothing \ll l$). The CZA curve may then be parametrized by the angle $\phi \in [-\pi/2, \pi/2]$, see Fig. 3(c), as

$$\begin{pmatrix} x \\ y \end{pmatrix} = l \tan e''_c \begin{pmatrix} \sin \phi'' \\ \cos \phi'' \end{pmatrix}, \quad (3)$$

wherein $\phi'' = \phi''(\phi)$, or $\sin(\phi'' + \phi) = n' \sin(\phi)$. Equation (3) describes a circle of radius $l \tan e''_c$, shown as a dashed line in Figs. 2(b) and 2(c). However, it turns out that only a segment of the circle is attainable by the exiting rays due to the occurrence of total internal reflection. The solid black line in Fig. 2(c) shows this limit. The critical internal angle of incidence may be found from $\phi_{\text{TIR}} = \arcsin(1/n')$, such that $\phi' = \pi/2$ marks the onset of total internal reflection. Herein n' is a function of e' , which is a function of e . One finds^{12,15}

$$\phi_{\text{TIR}} = \arccos\left(\frac{\sqrt{n_0^2 - 1}}{\cos e}\right), \quad (4)$$

which translates into a corresponding azimuthal limit $\phi''_{\text{TIR}} = \pi/2 - \phi_{\text{TIR}}$ of the (projected artificial) CZA.

A similar reasoning leads to the existence of a critical elevation angle e_{TIR} above which the internal second refraction becomes a total internal reflection, $e''_c = 0$ in Eq. (2). Equivalently, one may set $\phi_{\text{TIR}} \rightarrow 0$ and solve Eq. (4) for e to obtain^{11–13,15}

$$e_{\text{TIR}} = \arccos(\sqrt{n_0^2 - 1}). \quad (5)$$

Equation (5) shows that at around $e_{\text{TIR}} = 28^\circ$ even the last glimpse of the red, with index $n_0(\text{red}) = 1.332$, is less refracted than blue, with index $n_0(\text{blue}) = 1.341$, so part of the artificial (water) CZA disappears. For ice, taking $n_0 = 1.31$, the corresponding critical solar elevation above which this halo can no longer be observed is 32° .^{11–15} Equation (5) also shows that any material with $n_0 > \sqrt{2}$ (such as glass) will not produce a CZA (nor a CHA).^{19,33–35} For this reason alone, and in order to not have to construct a water-filled hexagonal prism, it is nice to have a simple analog demonstration experiment to overcome this practical limitation. The full azimuthal width of the CZA is $\Delta\phi''_{\text{CZA}} = 2\phi''_{\text{TIR}}$ and is an increasing function of the elevation, starting from 125° and approaching a half-circle, or 180° , for $e \rightarrow e_{\text{TIR}}$. In this limit, Eqs. (4) and (5) show that light emerges only from a small section around $\phi = 0$, where the effective index of refraction diverges $n'(e_{\text{TIR}}) \rightarrow \infty$ whereby the exiting refraction deviates rays at a right angle $\phi' \approx \pi/2$ towards the left and the right.

The complementary angle e''_c of the final exit ray's inclination, Eq. (2), corresponds to the angular distance to the azimuth of the natural CZA halo phenomenon.^{22–24} This angular distance is independent of the azimuth ϕ'' (or ϕ), such that the natural CZA appears as a true circle around the zenith, as shown in Fig. 2(a),^{12,13,15} just as the artificial CZA is a circle in the xy -plane, as shown in Fig. 2(b). One may also observe (both in natural displays of the phenomenon as well as in the experiment) that the angular width of the visible spectrum, or the chromatic angular dispersion $\Delta e''_c$

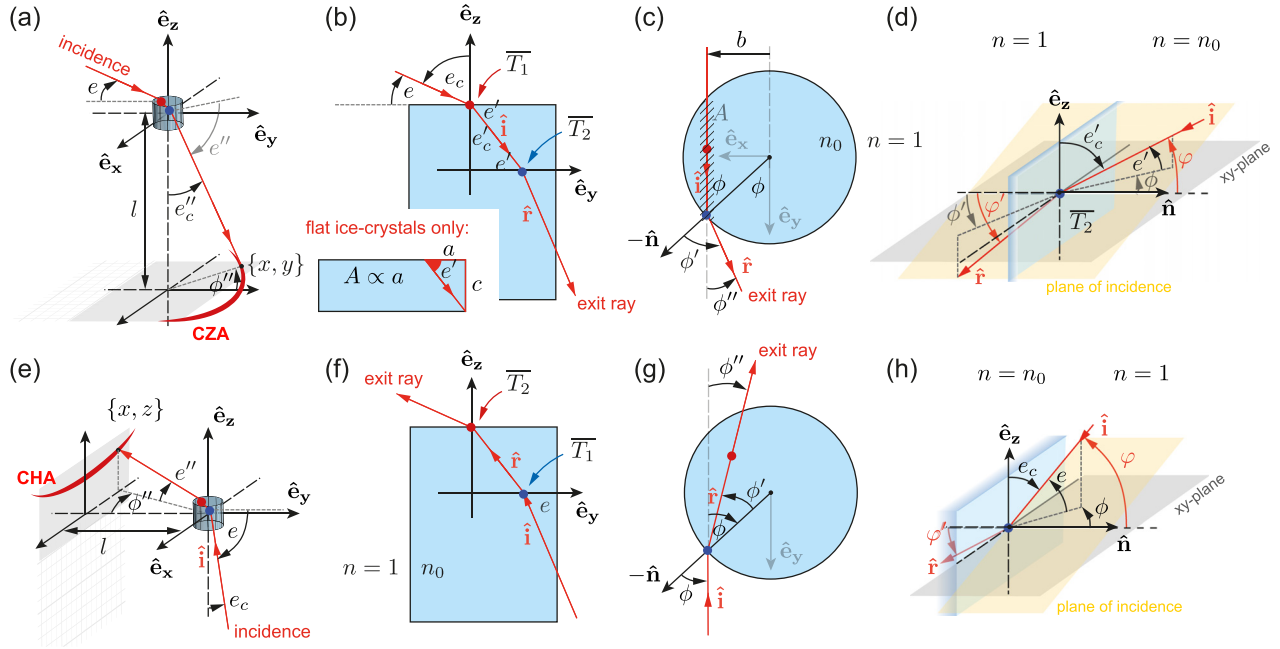


Fig. 3. Geometry and setup for the CZA experiment [panels (a)–(d)] and the CHA experiment [panels (e)–(h)]. See text for details.

$= e''_c(\text{red}) - e''_c(\text{blue})$, remains roughly constant at 1.6° (which may be compared to the dispersion $\sim 1.2^\circ$ and 2.2° of the primary and secondary rainbows, respectively). Only at very small inclination angles is a broadening observed^{11,15} before the shrinking CZA eventually disappears as it converges towards the zenith (or the point below the cylinder), cf. Figs. 2(a) and 2(c).

All of the above characteristics of the CZA can be readily observed with a focusable flashlight in hand and a glass of water resting at the edge of a table. For instance, by slowly lowering the incidence light direction on the water surface (while keeping aim by observing the shadow), the CZA can be seen to only emerge when the angle gets below 28° , starting with a wide and weak arc of small radius and good spectral separation below the glass, to then transition to a brighter but forwardly more confined arc, to then eventually disappear as a faint arc of largest radius, as shown in Fig. 2(c).

III. ARC INTENSITY

Without treating the situation in full detail, a description of the approximate intensity along the azimuthal coordinate ϕ'' requires several key factors to be considered including:^{11,18} T_1 , the transmission at the first interface; T_2 , the transmission at the second interface; the fact that $A \propto \cos \phi \sin e \cot e'$, a geometric factor;²⁵ $(d\phi''/db)^{-1}$, a ray bundling factor with $b = \sin \phi$ (see below); $(de''/dn_0)^{-1}$, a chromatic dispersion factor; and I_{AM} , atmospheric attenuation (for natural halos only).

The cross-sectional factor A takes the projected surface of the top face into account, which admits refraction along the ray path described by the internal angle ϕ , see dashed area in Fig. 3(c).^{25,26} The ray bundling factor is a caustic intensity factor for the cylinder experiment, and a fake caustic intensity factor for the natural counterpart.²⁰ Its concept is similar to that of the rainbow caustic,²⁷ and accounts for the predominance of certain deflection directions as outcomes of the refraction of an incident parallel bundle of rays. The fact that more rays experience a small azimuthal in-plane

refraction is then captured by this factor peaking around $\phi'' \approx 0$. However, in this case, no divergence of the intensity appears (meaning this factor remains finite at all times). The chromatic dispersion factor accounts for the changing width $\Delta e''_c \approx (de''/dn_0) \times [n_0(\text{blue}) - n_0(\text{red})]$ of the arc, such that its apparent brightness is $\propto 1/\Delta e''_c$. Overall then,

$$I(\phi'', e) \propto T_1 T_2 A (d\phi''/db)^{-1} (de''/dn_0)^{-1}, \quad (6)$$

which is plotted in Fig. 4. This expression quantifies the observed azimuthal decay in intensity away from the forward direction and towards zero for $\phi'' \rightarrow \phi''_{\text{TIR}}$ due to the second interface's transmission going smoothly to zero as the limit of total internal reflection is reached. The transmission coefficient $T_2(\phi)$ [blue dashed line in Fig. 4(a)], upon the second refraction, depends on the actual angle ϕ to the normal, as seen in Fig. 3(d), which is given by²⁹ $\phi = \arccos(\cos \phi \cos en_0^{-1})$. The parametric curves in Fig. 2(c) have been shaded according to this overall intensity function and match the appearance of experimentally observed CZAs projections and natural halo displays quite well. Together with the theoretical CZA azimuthal width $\Delta \phi''_{\text{CZA}}$, the above considerations quantify and reiterate the often-stated rule of thumb that a natural CZA rarely appears to exceed a quarter of a full circle.

Plotting the intensity in the forward direction at the position of maximum CZA intensity (at $\phi'' = \phi = 0$) as a function of the elevation (inclination), $I(e)$, one observes a wide peak, as seen by the thick black line in Fig. 4(b). This means that for some solar elevations (or light source inclinations) the (artificial) CZA is brighter as compared to others. For water and ice (including the atmospheric attenuation), this peak occurs at around 17° and 20° , respectively. For ice then, this value corresponds to the solar elevation at which the CZA is best observable in nature (see, for instance, Refs. 7, 11, 13, and 15). For water, this is the light source inclination for which the experiment produces the brightest CZA projection. Both T_1 (thin gray dashed line) and the geometric factor (thin gray solid line) describe the decay towards $e \rightarrow 0$. For the natural halo, the

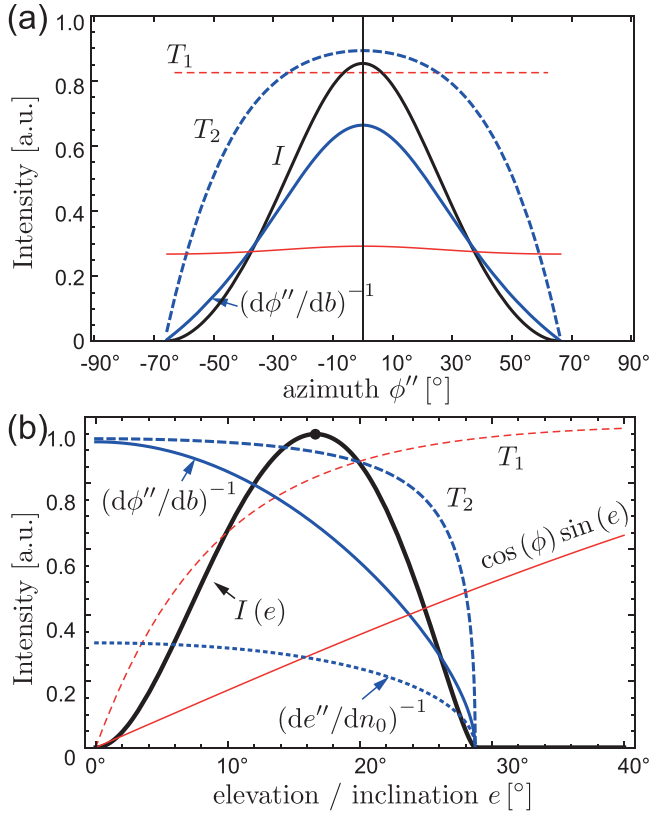


Fig. 4. (a) The (artificial) CZA intensity distribution along the azimuth coordinate ϕ'' at $e = 17^\circ$. Only for $\phi'' \in [-\phi''_{\text{TIR}}, +\phi''_{\text{TIR}}]$ is $I(\phi'') > 0$. (b) The CZA intensity at $\phi'' = 0$ for different elevation (inclination) angles e . Only for $e \in [0, e_{\text{TIR}}]$ is $I(e) > 0$ and the CZA observable. The refractive index of water (1.33) was used here; the picture for ice is very similar.

atmospheric attenuation also affects the decay when the sun is low and dim.²⁸ At the other end of the curve, T_2 (thick gray dashed line) along with the ray bundling factor (thick gray solid line) describe the decay towards $e \rightarrow e_{\text{TIR}}$. The decrease of the ray bundling factor may be understood as follows. The inclination angle e' increases for increasing elevation angles e such that the effective index of refraction n' of Eq. (1) increases as well (eventually diverging as we have seen). This in turn causes the exit rays, which are deflected by ϕ'' , to sweep more rapidly across the forward ($\phi'' = 0$) direction as the impact parameter b crosses the symmetry axis. Accordingly then, the bundling of rays in the forward direction is reduced as e increases.

IV. ARTIFICIAL CIRCUMHORIZONTAL ARC

We now turn to the artificial CHA, as shown in Fig. 5(a), for which the first refraction is at the side wall of the cylinder in the experiment, as seen in Figs. 3(e)–3(g). Thus, it is this refraction that must be treated according to the inclined skew-ray theory of Bravais. Again, we decompose the problem into two parts. The material's index of refraction n_0 directly determines the change in the inclination angle, $\sin e = n_0 \sin e'$, and the in-plane azimuthal refraction (i.e., as seen from above) follows $\sin \phi = n' \sin \phi'$, with the effective index of refraction being^{12–15,19,20}

$$n' = \sqrt{\frac{n_0^2 - \sin^2 e}{\cos^2 e}}. \quad (7)$$

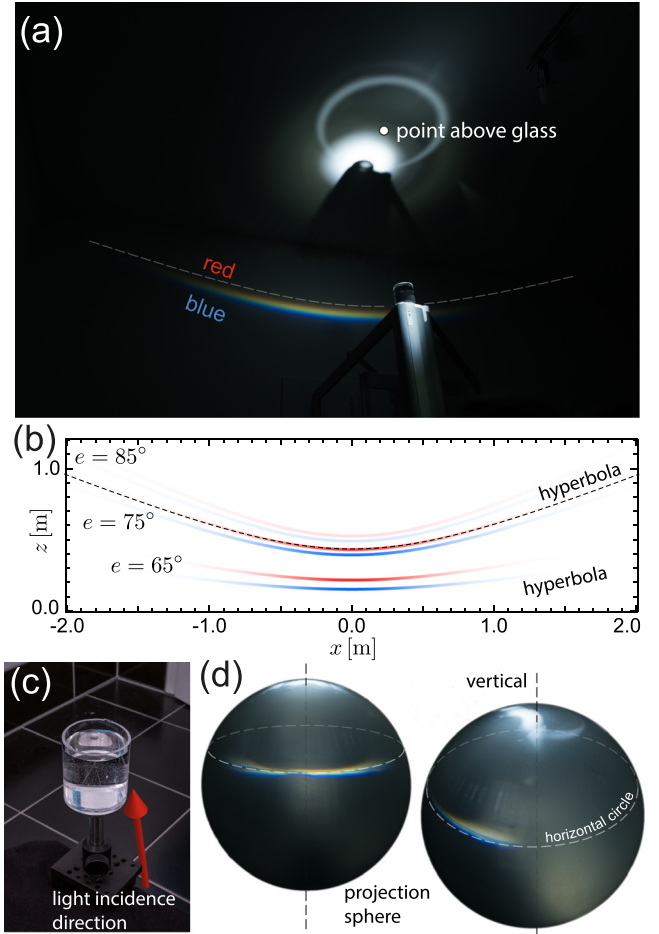


Fig. 5. (a) Artificial circumhorizontal arc (CHA) projection. The circle at the ceiling, crossing the shadow of the water-filled cylinder, corresponds to the natural parhelic circle halo (the external reflection contribution). (b) Plot of the CHA curve, Eq. (8), for elevations $e = \{65^\circ, 75^\circ, 85^\circ\}$ and for both red and blue ($l = 1$ m). (c) The acrylic cylinder as placed in the center of a spherical projection screen (Ref. 31). (d) Two views showing the CHA projection onto the spherical screen.

The second refraction at the top water-air interface only changes the inclination towards the horizontal, $n_0 \sin e'_c = \sin e''$, and no in-plane refraction takes place since the refracting interfaces' normal is vertical. One finds $\cos^2 e'' = n_0^2 - \sin^2 e$, which is the analog of Eq. (2). Referring to the experiment's setup and coordinates as defined in Figs. 3(e)–3(g), the curve (x, z) described by the artificial CHA on the vertical wall is parametrized by the angle ϕ as

$$\begin{pmatrix} x \\ z \end{pmatrix} = \frac{l}{\cos \phi''} \begin{pmatrix} \sin \phi'' \\ \tan \phi'' \end{pmatrix}, \quad (8)$$

where $\phi'' = \phi - \phi'$. Since $z^2 = (x^2 + l^2) \tan^2 e''$, and $\tan^2 e''$ is a constant (independent of x),³⁰ the artificial projected CHA for each inclination e is a hyperbola in the xz -plane, as seen in Fig. 5(b). If the projection were onto a sphere, the natural CHA halo's geometry of a circle segment parallel to the horizon (i.e., at constant elevation) were to be recovered, as discussed in Ref. 31 and Figs. 5(c) and 5(d).

The angle to the surface normal, which determines the transmission coefficient $T_1(\phi)$, is $\phi = \arccos(\cos \phi \cos e)$, as seen in Fig. 3(h). The transmission coefficient $T_2(e'_c)$

corresponds to the second refraction changing the elevation only. The intensity may then be analyzed along the same lines as for the CZA, but with the cross-sectional factor being $\cos \phi \cos e$.³⁶ Again, this approach was used to set the transparency of the curves in Fig. 5(b). We find that the CHA is brightest at around $e = 69^\circ$ in the experiment and 65° for the natural halo, whereas azimuthally it decays to zero for $\phi \rightarrow \pi/2$ (grazing incidence) where accordingly $\phi'' = \pi/2 - \arcsin(1/n')$.^{12,15} The corresponding full azimuthal width $\Delta\phi''_{\text{CHA}}$ of twice that value therefore ranges from $125^\circ \rightarrow 180^\circ$ in the experiment and $116^\circ \rightarrow 180^\circ$ for the natural ice halo phenomenon. The half-circle limit is reached in the reverse situation as compared to the CZA (here for grazing incidence with $e = \pi/2$, as compared to grazing exit $e'' = \pi/2$ for the CZA). The natural CHA only forms when the inclination is larger than $\pi/2 - e_{\text{TIR}} = 58^\circ$ (ice¹⁵) and 62° (water), where the critical inclination as determined for the CZA, in Eq. (5), can be reused. The halo rises in altitude (elevation) as the sun approaches the zenith (90° angle of incidence onto the side face), where it will be $e'' = 32^\circ$.^{12,14} The experimental CHA reproduces these behaviors closely.

V. CONCLUSION AND OUTLOOK

We have argued that a very simple experiment, namely, a glass filled with water illuminated under various directions of incidence, provides a rich phenomenology. We have shown that the emerging projections of light closely correspond to two natural atmospheric ice halos: the circumzenithal and the circumhorizontal arcs. The general angular characteristics derived and validated by the experiment also apply to their natural counterparts. This demonstration experiment may complement more complex ones based on spinning glass crystals.^{19,31–35} It also produces a purer spectrum as compared to a rainbow demonstration experiment since, similar to the action of a prism, ideally no color-overlap occurs. The experiment may be used as a halo alternative to popular rainbow demonstrations,⁵ as an illustrative example of skew-ray refraction, or simply to show dispersion.

We end with an outlook on similar experiments. One may use a water-filled martini cocktail glass as a refracting cone, as shown in Fig. 6. By the same idea that led us to the CZA analogy, one may confirm (see Appendix B) that the average geometry of light entering through the top air-water interface and leaving through the lateral cone surface results in an analogy to Parry's halo.^{6,8,15} Using a cocktail glass, one may find in addition an artificial parhelic circle due to external

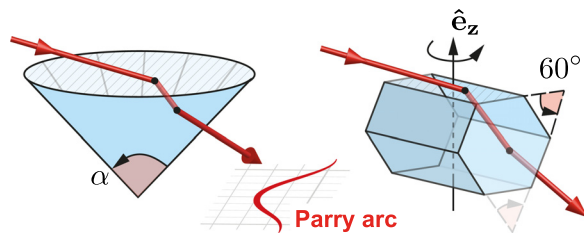


Fig. 6. Analogy (in the sense of Fig. 1) of the parallel light refraction by a cone (e.g., a filled martini glass) and the ray path responsible for the upper suncave Parry arc (Refs. 6, 8, and 15). While the martini glass typically has an apex angle of $\alpha \sim 70^\circ$ instead of the 60° required for a perfect analogy, the resulting pattern is very similar. Best results are obtained when a slit-aperture is used to constrain illumination to a band across the diameter only.

reflections from the stem of the glass as well as artificial heliac arcs⁸ due to external reflections by the conical surface. Also, placing an opaque obstacle inside the glass of water of the original experiment, a parhelicion-like appearance can be obtained.³⁹ Likely, many more halo counterparts may be realized along the lines presented here.

APPENDIX A: COLORS

Throughout the article the computations focused mainly on the shape of the artificial halos. This appendix shall briefly outline how the visual color perception of either artificial or natural halos may be described. Perceived colors can be computed as follows. First, the tristimulus values (trichromatic color space coordinates) $\{X, Y, Z\}$ are computed via the CIE standard colorimetric observer color matching functions $\{\bar{x}, \bar{y}, \bar{z}\}$ and from the spectral radiance L , via, e.g., $X = \int_0^\infty L(\lambda)\bar{x}(\lambda) d\lambda$. We assumed a linear relation between this quantity and the spectral power density of a given light source. For a single wavelength, a narrow (FWHM ~ 1 nm) Gaussian line spectrum was chosen. Then, a linear transformation (a matrix product) converts these to linear RGB values, $(R_L, G_L, B_L) = M \cdot (X, Y, Z)$, which subsequently are converted to the common sRGB color space values through a non-linear transformation. Finally, the values are normalized to give a valid sRGB color. The required data can be found online.³⁷ The hereby obtained sRGB color values $\{R_s, G_s, B_s\}$ for each wavelength were multiplied by an intensity factor I/I_0 to recreate the azimuthal intensity decay of the correspondingly colored CZH segments corresponding to $n_0(\lambda)$.

Corresponding computations assuming a solar spectrum, a LED light source spectrum, and an incandescent light bulb spectrum along with the dispersion $n_0(\lambda)$ of water are shown in Fig. 7 for different elevations. These images can be compared to experiments or displays computed with dedicated halo simulation software.³⁸ Note that in the experiment colors may superimpose (and green disappear) if the projection distance l is too small.

APPENDIX B: ARTIFICIAL SUNCAVE PARRY ARC

We keep the notation of Fig. 3(a), where we imagine the cylinder being replaced by the cone of Fig. 6, and acknowledge that for the second refraction (the first being analogous to the CZA) the normal vector is now $\hat{\mathbf{n}} = (-\cos(\alpha/2) \sin \phi, -\cos(\alpha/2) \cos \phi, \sin(\alpha/2))$ for the cone's lateral surface. The incidence direction vector $\hat{\mathbf{i}} = (0, \sin e'_c, -\cos e'_c)$ makes an angle $\varphi = \arccos(-\hat{\mathbf{i}} \cdot \hat{\mathbf{n}})$ to this normal. The refracted angle is then determined by $n_0 \sin \varphi = \sin \varphi'$. To get the refracted ray, one may rotate the external unit vector $-\hat{\mathbf{n}}$ according to the right hand rule by φ' about an axis perpendicular to the plane of incidence, defined by the unit vector $\hat{\mathbf{k}} = \hat{\mathbf{i}} \times \hat{\mathbf{n}} / \sin \varphi$. This can be done via Rodrigues' rotation formula, yielding the exiting ray's unit direction vector $\hat{\mathbf{r}} = (\hat{r}_x, \hat{r}_y, \hat{r}_z) = \hat{\mathbf{n}}(n_0 \cos \varphi - \cos \varphi') + \hat{\mathbf{i}} n_0$. The line described by this unit direction vector and starting at a height l above the origin (at the position of the glass) intersects the horizontal xy -(projection-)plane at the point $(x, y, 0) = l\hat{\mathbf{e}}_z - l\hat{\mathbf{r}}/\hat{\mathbf{e}}_z \cdot \hat{\mathbf{r}}$. This is the artificial projected suncave Parry arc^{6,8,15} parameterized by ϕ .

The complementary angle to the elevation is $e''_c = \arccos(-\hat{\mathbf{e}}_z \cdot \hat{\mathbf{r}})$ when $\hat{r}_y > 0$, and negative that value when $\hat{r}_y < 0$, signifying a Parry arc beyond the zenith with e''

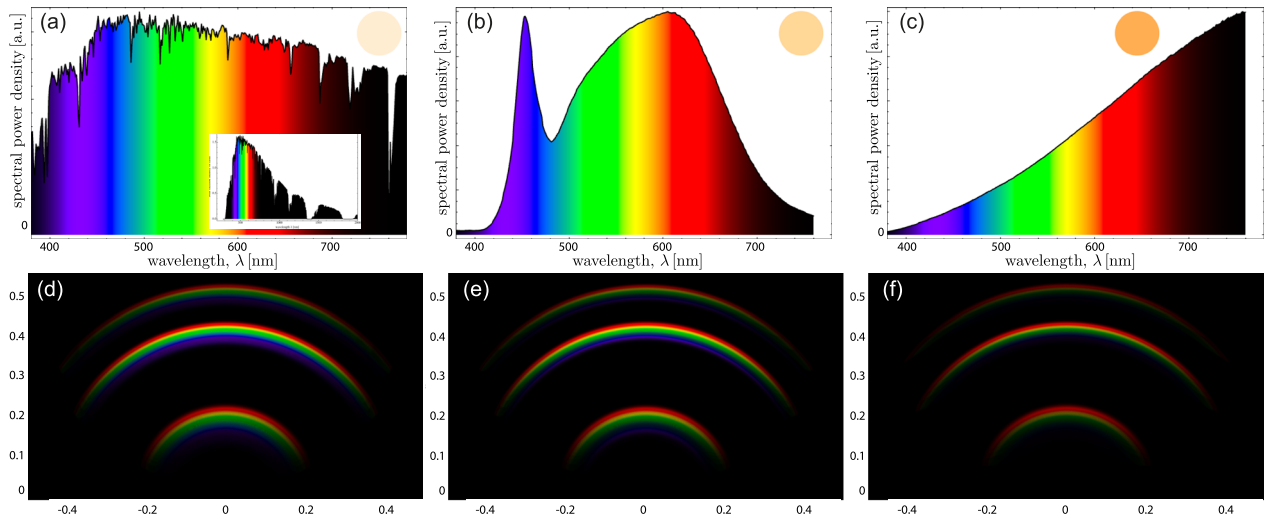


Fig. 7. Light source spectral power densities for (a) sun light, (b) LED light, and (c) incandescent light bulb. The colors of the sources are shown in the spectrum's insets. Panels (d)–(f) give the corresponding perceived colors of the artificial CZAs in the xy -plane.

$> \pi/2$ (in front of the cocktail glass when viewed from the direction of incident light). The azimuths are $\phi'' = \pm \arccos((0, 1, 0) \cdot (\hat{r}_x, \hat{r}_y, 0) / |(\hat{r}_x, \hat{r}_y, 0)|)$, where the plus sign applies to $\hat{r}_x < 0$ and the negative sign to $\hat{r}_x > 0$. The arc appears concave towards the shadow of the glass (corresponding to the sun position and being suncave as its natural counterpart), and the angular distance to this shadow, $\Delta_S = \arccos((0, \cos(e), -\sin(e)) \cdot \hat{r})$, corresponds to the distance to the sun for the natural halo. The hereby obtained angular coordinates agree with those in Ref. 15. Alternatively then, the projected artificial Parry arc curve on the floor may be computed via Eq. (3) if the following replacements via the variables of Wegener's¹⁵ chapter 12 are made: $e''_c \rightarrow \pi/2 - h_\sigma$ and $\phi'' \rightarrow \delta$ and Wegener's φ being the parametrization. Using glasses with smaller apex angles α (walls becoming increasingly vertical and more cylinder-like), the arc inverts from suncave to sunvex and approaches the CZA in the limit $\alpha \rightarrow 0$.

^aElectronic mail: markus.selmke@gmx.de; URL: <http://photonicsdesign.jimdo.com>
¹C. J. Lynde, *Gilbert Light Experiments for Boys* (The A. C. Gilbert Co., New Haven, Conn., 1920), Experiment No. 94.
²M. Edgeworth and R. L. Edgeworth, *Practical Education* 1, 55–56 (Printed for J. Johnson, St. Paul's Church-Yard, London, 1798).
³D. Ivanov and S. Nikolov, "Optics demonstrations using cylindrical lenses," *Phys. Educ.* **50**(5), 548–559 (2015).
⁴M. Selmke and S. Selmke, "Revisiting the round bottom flask rainbow experiment," *Am. J. Phys.* (submitted).
⁵G. Casini and A. Covello, "The 'rainbow' in the drop," *Am. J. Phys.* **80**(11), 1027–1034 (2012).
⁶R. Greenler, *Rainbows, Halos and Glories* (Cambridge U.P., England, 1980).
⁷L. Cowley, website "atmospheric optics," <<http://www.atoptics.co.uk/halosim.htm>>.
⁸W. Tape, *Atmospheric Halos*, Antarctic Research Series (American Geophysical Union, Washington, D.C., 1994).
⁹W. Tape and J. Moilanen, *Atmospheric Halos and the Search for Angle x* (American Geophysical Union, Washington, D.C., 2006).
¹⁰M. Minnaert, *The Nature of Light and Color in the Open Air* (Dover, New York, USA, 1954).
¹¹R. S. McDowell, "Frequency analysis of the circumzenithal arc: Evidence for the oscillation of ice-crystal plates in the upper atmosphere," *J. Opt. Soc. Am.* **69**(8), 1119–1122 (1979).

¹²A. Bravais, "Mémoire sur les halos et les phénomènes optiques qui les accompagnent," *J. de l'École Royale Polytech.* **31**(18), 1–270 (1847).
¹³W. J. Humphreys, *Physics of the Air*, 2nd ed. (McGraw-Hill Book Company, Inc., New York and London, 1929).
¹⁴R. A. R. Tricker, *Introduction to Meteorological Optics* (Mills & Boon, London, 1970).
¹⁵A. Wegener, *Theorie der Haupthalos* (L. Friederichsen & Co, Hamburg, 1926).
¹⁶The distance must be much larger than the focal distance of the curved cylinder interface, $f = Rn'/(n' - 1)$, where R is the cylinder's radius. Practically speaking, a distance $\geq 10R$ is fine.
¹⁷Huygens (Ref. 18) hypothesized horizontal cylindrical of arbitrary in-plane orientation to describe what was at that time thought to be a tangent arc to the 46° circular halo (Refs. 9 and 24).
¹⁸C. Huygens, *Oeuvres Complètes Tome XVII: L'horloge à pendule de 1651 à 1666. Travaux divers de physique, de mécanique et de technique de 1650 à 1666. Traité des couronnes et des parhélies (1662 ou 1663)* (ed. J.A. Vollgraff. Martinus Nijhoff, Den Haag, 1932); see arc THS in Fig. 22, §37, and its discussion.
¹⁹M. Selmke, "Artificial Halos," *Am. J. Phys.* **83**(9), 751–760 (2015).
²⁰G. P. Können, "Polarization and intensity distributions of refraction halos," *J. Opt. Soc. Am.* **73**(12), 1629–1640 (1983).
²¹Usually, the effective index of refraction n' is discussed for rays entering a dense material from air, as given in Eq. (7) (Refs. 12–14 and 19). For the inverse situation, note that refraction from $n = n_0$ to $n = 1$ is mathematically equivalent to refraction from $n = 1$ into $n = 1/n_0$. Equation (1) follows by inverting the corresponding effective inverse index of refraction, $[(1/n_0)]^{-1}$.
²²Wolfram Alpha, Wolfram Alpha LLC, <[http://www.wolframalpha.com/input/?i=solar+elevation,+51.33065N,12.37595E,+24.10.2015,+1:04pm](http://www.wolframalpha.com/input/?i=solar+elevation,+51.33065N,12.37595E,+24.10.2015,+1:04pm;)>; retrieval date: 07/2005/2016.
²³The ratio $r = D/w = 0.347$, where D is the CZA diameter and w is the image width, may be used to extract the angular distance to the zenith, $e''_c = \arctan(rX/2f) = 16^\circ$. This value is in agreement with Eq. (2), $e = 27^\circ$ (Ref. 22) and $n = 1.31$. The focal length of the rectilinear projection lens was $f = 14$ mm and $X = 23.6$ mm the APS-C sensor's x -dimension.
²⁴For the natural halo, the exit angle's altitude e'' is close to tangential (Ref. 12) to the circular 46° halo, i.e., $e + D_m$, where $D_m = 2\arcsin[n_0 \sin(A/2)] - A$ is the minimum deviation angle through a $A = 90^\circ$ prism. However, it is not precisely equal (Refs. 13 and 14) except for $e = \arccos(n_0/\sqrt{2}) = 22^\circ$.
²⁵The factor $\cot e'$ only appears in case of the natural flat hexagonal plate crystals, see Ref. 11. We also neglect statistical misalignments of the ice crystals, cf. Refs. 9 and 18.
²⁶R. S. McDowell, "The formation of parhelia at higher solar elevations," *J. Atmos. Sci.* **31**(7), 1876–1884 (1974).
²⁷M. V. Berry, "Nature's optics and our understanding of light," *Contemp. Phys.* **56**(1), 2–16 (2015).

- ²⁸Air mass (solar energy), from Wikipedia, the free encyclopedia, <[https://en.wikipedia.org/wiki/Air_mass_\(solar_energy\)](https://en.wikipedia.org/wiki/Air_mass_(solar_energy))>; retrieval date (March 08, 2016), $I_{AM} \propto 0.7^{AM^{0.678}}$, $AM(e)$: spherical shell approximation.
- ²⁹To see this, consider the dot product $\cos \phi = -\hat{\mathbf{i}} \cdot \hat{\mathbf{n}}$ of the incidence ray's unit vector $\hat{\mathbf{i}} = (0, \sin e'_c, -\cos e'_c)$ and the cylinder surface normal $\hat{\mathbf{n}} = (-\sin \phi, -\cos \phi, 0)$ at the point of refraction, as shown in Figs. 3(a)–3(d)
- ³⁰Figures 3(e)–3(h) show that $\tan e'' = z/\rho$, $\sin \phi'' = x/\rho$, and $\cos \phi'' = l/\rho$, where $\rho^2 = l^2 + x^2$.
- ³¹M. Selmke and S. Selmke “Complex artificial halos for the classroom,” *Am. J. Phys.* **84**(7), 561–564 (2016).
- ³²M. Vollmer and R. Greenler, “Halo and mirage demonstrations in atmospheric optics,” *Appl. Opt.* **42**(3), 394–398 (2003).
- ³³M. Vollmer and R. Tammer, “Laboratory experiments in atmospheric optics,” *Opt. Express* **37**(9), 1557–1568 (1998).
- ³⁴M. Großmann, K.-P. Moellmann, and M. Vollmer, “Artificially generated halos: Rotating sample crystals around various axes,” *Appl. Opt.* **54**(4), B97–B106 (2014).
- ³⁵S. Borchardt and M. Selmke, “Intensity distribution of the parhelic circle and embedded parhelia at zero solar elevation: Theory and experiments,” *Appl. Opt.* **54**(22), 6608–6615 (2015).

- ³⁶To include the effect of the reduced projection intensity on the wall due to the inclination of the rays, one may further include a factor $\sim \cos \phi''$. We choose to ignore it here to be in line with the natural CHA intensity.
- ³⁷See, for example, the international commission on illumination, <<http://www.cie.co.at>> and Wikipedia, <<https://en.wikipedia.org/wiki/SRGB>>.
- ³⁸L. Cowley and M. Schroeder, HaloSim simulation program; <<http://www.atoptics.co.uk/halo/halfeat.htm>>.
- ³⁹The deflection through a cylinder of radius R_2 with an inner (centered) opaque cylindrical obstacle of radius R_1 is $\Delta = 2(\alpha - \beta)$, where α and β are the incidence and refracted angles, respectively, related by $\sin \alpha = n' \sin \beta$. The symmetrical geometry of the corresponding least-deflected ray touching the inner cylinder tangentially shows that $\sin \beta = R_1/R_2$. Demanding that its deflection equals the actual prismatic angle of minimum deviation (the parheliion azimuth) (Ref. 24), $D_m(n') = \Delta$, one finds after lengthy algebra, $\sin^2 \alpha = n'^2 \sin^2(A/2)$ (here, $A = 60^\circ$). Using this solution yields $R_1/R_2 = 1/2$. Illuminating (through the side walls) a filled glass with half its interior blocked produces thus a parheliion-like projection and represents the (false) mechanism Huygens conceived of (Ref. 7 and 16). It is thus *not* an analog of the actual parheliion mechanism (Refs. 6–10 and 12–15).



Gilley Gramme Machine

This demonstration generator, in the collection of the Williston-Northampton School in Easthampton, Massachusetts, is listed at \$7.75 in the 1916 catalogue of the L.E. Knott Apparatus Company of Boston. The flat design enables the students to place a sheet of glass over the armature and the field magnet and trace out the magnetic lines of force using iron filings. The apparatus showed the design of a popular form of generator of the era. Today almost all technology has disappeared from high school and college physics courses, and we would not find a place for the apparatus in our collections. (Picture and Notes by Thomas B. Greenslade, Jr., Kenyon College)